## Optimizing sparse quantum state preparation with measurement and feedforward

Yao-Cheng Lu<sup>©\*</sup> and Han-Hsuan Lin<sup>©†</sup>

Department of Computer Science, National Tsing Hua University, Hsinchu 300044, Taiwan

Quantum state preparation (QSP) is a key component in many quantum algorithms. In particular, the problem of sparse QSP (SQSP) — the task of preparing the states with only a small number of non-zero amplitudes — has garnered significant attention in recent years. In this work, we focus on reducing the circuit depth of SQSP with limited number of ancilla qubits. We present two SQSP algorithms: one with depth  $O(n \log d)$ , and another that reduces depth to O(n). The latter leverages mid-circuit measurement and feedforward, where intermediate measurement outcomes are used to control subsequent quantum operations. Both constructions have size O(dn) and use O(d) ancilla qubits. Compared to the state-of-the-art SQSP algorithm in Sun et al., IEEE, 2023, which allows an arbitrary number of ancilla qubits m > 0, both of our algorithms achieve lower circuit depth when m = d.

## I. INTRODUCTION

#### A. Motivation

Since the advent of quantum computing, numerous quantum algorithms have been developed, demonstrating significant speedups over classical algorithms. [1, 2] A fundamental step in many algorithms — such as variational quantum algorithms [3], hybrid quantum-classical Monte-Carlo methods [4, 5], and quantum linear solvers [6, 7] — is the initialization of classical data on a quantum device. Furthermore, some algorithms [8] may require reinitializing the quantum state multiple times during execution. Quantum state preparation is a particularly important step in these algorithms and can often dominate the overall run time. Therefore, efficiently preparing quantum states is a critical challenge in quantum computing.

The asymptotically optimal bounds for the depth complexity of the general quantum state preparation (GQSP) without ancilla qubits is  $\Theta\left(\frac{2^n}{n}\right)$  [9]. When ancilla qubits are available, the trade-offs depend on the number of ancilla qubits used. With m ancilla qubits, if  $m = O(\frac{2^n}{n \log n})$ , the circuit depth can be reduced to  $\Theta(\frac{2^n}{n+m})$ . If  $m = \Omega(2^n)$ , the circuit depth can be further reduced to  $\Theta(n)$ . Both bounds asymptotically optimal [9]. When the number of ancilla qubits is within the range  $\omega(\frac{2^n}{n \log n})$  to  $o(2^n)$ , the circuit depth ranges between  $\Omega(n)$  and  $O(n \log n)$  [9]. All GQSP algorithms require a circuit size of  $\Theta(2^n)$ , which demands substantial computational resources [10].

Due to the high cost of preparing a general quantum state, several works have focused on designing QSP algorithms for states with specific structures that arise from particular applications, such as uniform quantum states [11], low-rank quantum states [12], and cyclic quantum states [13]. Leveraging these structures allows for a more efficient generation of quantum states.

The sparse quantum states, quantum states with few non-zero amplitudes, are another category of quantum states with specific structure and practical applications. Bell states [14, 15], thermofield double states [16], W states [17], Dicke states [18], and GHZ states [15] all fall into this category. Sparse quantum states have applications in several algorithms, such as quantum Byzantine agreement algorithm [19]. The problem of sparse quantum state preparation (SQSP) has been studied extensively recently [9, 20–29]. In this work, we focus on solving the SQSP problem, aiming to minimize the resources required.

Definition 1. (SQSP Problem) Given two positive integers n and  $0 < d \le 2^n$ , and a set S consisting of d tuples:

$$S = \{ (\alpha_i, q_i) \mid \alpha_i \in \mathbb{C}, q_i \in \{0, 1\}^n, 0 \le i < d \},$$
 (1)

where  $\sum_{i=0}^{d-1} |\alpha_i|^2 = 1$ . We define an *n*-qubit *d*-sparse state  $|\phi(n,d,S)\rangle$  as below:

$$|\phi(n,d,S)\rangle = \sum_{i=0}^{d-1} \alpha_i |q_i\rangle.$$
 (2)

Sometime we abbreviate  $|\phi(n,d,S)\rangle$  as  $|\phi\rangle$ . The goal of the SQSP problem is to generate an arbitrary sparse quantum state given n, d, S.

In the Noisy Intermediate-Scale Quantum (NISQ) era, both the circuit depth and the number of qubits play the critical roles in determining the feasibility of a quantum algorithm. Limited coherence time constrains the achievable circuit depth, while fewer qubits simplify hardware control and reduce error rates. In many SQSP algorithms, circuit depth compression relies on the use of parallel operations, which typically require additional ancilla qubits. However, this space-for-time trade-off can become impractical for target states with large n, where the number of ancilla qubits may scale linearly or more with n, making it difficult to balance circuit depth and qubit overhead.

To address this challenge, our first construction keeps

<sup>\*</sup> Contact author: yao.cheng.lu@gapp.nthu.edu.tw

<sup>†</sup> Contact author: linhh@cs.nthu.edu.tw

the number of ancilla qubits at O(d), which can be significantly lower than many prior algorithms, while maintaining circuit depth  $O(n \log d)$ . This offers a practical balance between depth and qubit usage, making our method particularly suitable for the case with limited qubit resources, especially when  $n \gg d$ , where either circuit depth or ancilla used can be significantly reduced compared to known algorithms (See Table I).

Furthermore, building upon the first algorithm, we incorporate measurement and feedforward to further reduce the circuit depth. By leveraging intermediate measurement outcomes to control subsequent quantum operations, our MaF-based construction achieves circuit depth O(n) that is independent of the sparsity d.

#### B. Measurement and feedforward

Measurement and feedforward is a quantum circuit design architecture that enables depth reduction by integrating mid-circuit measurements and classical feedforward to guide quantum operations. We denote  $\mathsf{MaF}(\mathcal{Q},\mathcal{C},l)$  as the class of circuit with measurement and feedforward consisting of l alternating quantum and classical layers. Each quantum layer is a quantum circuit in the class  $\mathcal{Q}$ , and each classical layer is a classical circuit in the class C. In this structure, quantum layers apply unitary operations and mid-circuit measurements on selected qubits. When mid-circuit measurements are performed, the measured qubits collapse to a definite classical state, while unmeasured qubits remain unaffected. The measurement results are first processed classically. and then used to apply conditional gates that control subsequent quantum operations. This dynamic adaptation enables circuits to adjust during execution, making quantum computations more flexible. In this work, we use MaF to abbreviate  $MaF(QPoly(n), NC^1, n)$ . We refer to a circuit within this framework as a MaF circuit. A formal definition of MaF will be provided in Chapter IIB.

MaF has a wide range of applications in quantum computing. For example, in quantum error correction [30], measurement outcomes determine the corrective steps needed to maintain fault tolerance. Similarly, in quantum teleportation [31], measurement outcomes are classically transmitted to a distant party, enabling reconstruction of the original quantum state. Furthermore, dynamic circuits with MaF have shown significant potential in the preparation of long-range entangled states [32].

In this work, the MaF-based design plays a crucial role in achieving efficient parallel execution. The algorithm involves extensive use of fan-out gates to enable parallel

operations and thereby speed up the circuit. By implementing these fan-out gates with a  $\mathsf{MaF}$  circuit, their depth can be minimized from logarithmic to constant with respect to the number of qubits of the target state. As a result, the overall circuit depth of the algorithm is reduced and made independent of the sparsity d.

#### C. Contributions and comparison

In this work, we study the SQSP algorithms and focus on optimizing the circuit depth and the number of ancilla qubits. We study two cases: without and with using a MaF circuit.

First, we give a construction without a MaF circuit:

Theorem 1. (SQSP algorithm) With the gate set drawn from  $\{U(2),CNOT\}$ , arbitrary n-qubit d-sparse quantum states can be prepared with a circuit of size O(dn), depth  $O(n \log d)$ , and O(d) ancilla qubits.

Compared to existing SQSP algorithms that use a constant number of ancilla qubits [20-24, 26-29], our algorithm achieves a lower circuit depth of  $O(n \log d)$ . While some SQSP algorithms attain lower circuit depth, such as [25] and [29], they require a much larger number of ancilla qubits— $O(dn \log d)$  and  $O(\frac{dn}{\log d})$ , respectively—which can in turn increase the total qubit requirements of the overall algorithm. In contrast, our algorithm achieves a reasonable circuit depth while using only O(d) ancilla qubits. Finally, although the algorithm in [9] supporting a trade-off with m ancilla qubits for any  $m \geq 0$ , our algorithm still achieves a lower circuit depth under the condition m = O(d).

While Theorem 1 presents an efficient construction without a MaF circuit, integrating MaF-based design into the construction allows us to achieve an even lower circuit depth. This leads to the following improved result:

Theorem 2. (SQSP algorithm with a MaF circuit) With the gate set drawn from  $\{U(2),CNOT\}$ , arbitrary n-qubit d-sparse quantum states can be prepared using a circuit of size O(dn), depth O(n), and O(d) acilla qubits within the class MaF(QPoly(n), NC<sup>1</sup>, n).

Compared to the constant-depth SQSP algorithm [33], our approach significantly reduces both the circuit size and the number of ancilla qubits. Moreover, since many algorithms using GQSP as a subroutine have O(n) circuit depths [34, 35], an SQSP algorithm with linear depth remains competitive in these cases.

The results of the two algorithms, along with comparisons to existing algorithms, are presented in Table I and Table II, respectively.

## D. Overview of algorithm

A SQSP algorithm can be implemented through various approaches. Some methods set computational basis states into correct amplitudes one by one by applying

<sup>&</sup>lt;sup>1</sup> QPoly(n) denotes the class of quantum circuits with polynomial size. We abuse the notation by using NC<sup>1</sup> to denote the class of classical circuit with logarithmic depth and polynomial size, rather than the corresponding class of decision problems.

| TABLE I. Comparison | of our result to | previous SQSP | methods without | a MaF circuit. |
|---------------------|------------------|---------------|-----------------|----------------|
|                     |                  |               |                 |                |
|                     |                  |               |                 |                |

| Algorithm | Circuit Size                                       | Depth                                  | #Ancilla                          |
|-----------|--|--|-----------------------------------|
| [20, 28]  | O(dn)  | O(dn)                                  | 0                                 |
| [29]      | $O\left(\frac{dn}{\log n} + n\right)$              | /                                      | 0                                 |
| [21-24]   | O(dn)  | O(dn)                                  | 1                                 |
| [26]      | $O\left(\frac{dn}{\log n} + n\right)$              | /                                      | 2                                 |
| [27]      | O(dn)  | /                                      | 2                                 |
| [29]      | $O\left(\frac{dn}{\log d}\right)$                  | $O(\log dn)$                           | $O\left(\frac{dn}{\log d}\right)$ |
| [25]      | $O(dn \log d)$                                     | $\Theta(\log dn)$                      | $O(dn \log d)$                    |
| [9]       | /  | $O(n\log dn + \frac{dn^2\log d}{n+m})$ | O(m)                              |
| [29]      | $\Omega\left(\frac{dn}{\log(m+n)+\log d}+n\right)$ | /                                      | $O(m)^{\mathrm{a}}$               |
| [29]      | $\Theta\left(\frac{dn}{\log dn} + n\right)$        | /                                      | unlimited number                  |
| Theorem 1 | O(dn)  | $O(n \log d)$                          | O(d)                              |

<sup>&</sup>lt;sup>a</sup> under the condition m = O(dn)

TABLE II. Comparison of our result to previous SQSP method with a MaF circuit.

| Algorithm | Circuit Size    | Depth       | #Ancilla        |
|-----------|-----------------|-------------|-----------------|
| [33]      | $O(d^2 \log n)$ | $\Theta(1)$ | $O(d^2 \log n)$ |
| Theorem 2 | O(dn)           | O(n)        | O(d)            |

many multi-controlled single-target gates [26], while others employ decision trees to perform the correct rotations on each of the n qubits sequentially [21]. In our work, we adopt a permutation-based strategy, as also employed in [23]. The core idea is to initially produce the correct amplitudes with  $\lceil \log d \rceil$  qubits, and then move each amplitude to its desired position. Below is a high-level overview of the algorithm. Let  $|\phi\rangle = \sum_{i=0}^{d-1} \alpha_i |q_i\rangle$  be the target quantum state. The first step uses the GQSP algorithm to prepare the state  $|\phi'\rangle$ :

$$|\phi'\rangle = \sum_{i=0}^{d-1} \alpha_i |i\rangle, \qquad (3)$$

whose amplitudes correspond to the non-zero entries of  $|\phi\rangle$  using only  $\lceil \log d \rceil$  qubits. In the next step, we first expand  $|\phi'\rangle$  to n qubits, and then apply a permutation unitary that maps  $|\phi'\rangle$  to  $|\phi\rangle$ . We can split this step into three individual steps: one-hot encoding, permutation and garbage elimination.

In the one-hot encoding step, we project d distinct entries onto d ancilla qubits:

$$\sum_{i=0}^{d-1} \alpha_i |i\rangle |0\rangle^{\otimes n - \lceil \log d \rceil} |0\rangle^{\otimes d} \longrightarrow \sum_{i=0}^{d-1} \alpha_i |i\rangle |0\rangle^{\otimes n - \lceil \log d \rceil} |e_i\rangle,$$
(4)

where  $|e_i\rangle$  denotes the quantum state in which the *i*th qubit is  $|1\rangle$ , while all other qubits are  $|0\rangle$ , known as the one-hot encoding of *i*. This allows next step to be executed in parallel, thereby minimizing circuit depth.

Next, we are entering the most pivotal phase known as permutation step. The purpose of this step is to position each amplitude in its appropriate position, in other words, to transform  $|i\rangle$  to  $|g_i\rangle$ :

$$\sum_{i=0}^{d-1} \alpha_i |i\rangle |0\rangle^{\otimes n - \lceil \log d \rceil} |e_i\rangle \longrightarrow \sum_{i=0}^{d-1} \alpha_i |q_i\rangle |e_i\rangle.$$
 (5)

The n qubits of  $|\phi'\rangle |0\rangle^{\otimes n-\lceil \log d \rceil}$  are processed in sequence. By controlling specific qubits of  $|e_i\rangle$ , we can determine whether each qubit will be flipped. To process all d basis states in parallel, we use a quantum OR-controlled single target X gate controlled by the one-hot state. The target qubit is flipped if any of the control qubits is  $|1\rangle$ . After completing this step, the desired state  $|\phi\rangle$  is now prepared in the first n qubits. Finally, the ancilla qubits need to be reset to 0. The circuit for executing this algorithm requires size O(dn), depth  $O(n \log d)$ , and O(d) ancilla qubits.

To further reduce the circuit depth, we adopt the Measurement and Feedforward (MaF) design [36]. It is a circuit design architecture that enables depth reduction by integrating mid-circuit measurements and classical feedforward to guide quantum operations. We adopt the constant-depth construction of arbitrary qubit fan-out gates from [37]. The fan-out gates used in the one-hot encoding step and garbage elimination step can be optimized using the constant-depth construction, thereby reducing the circuit depth. In the permutation step, due to the property established in Lemma 1, the quantum ORcontrolled X gate can be replaced by a parity-controlled X gate, which can be implemented using a fan-out gate and Hadamard gates. As a result, all three steps can leverage the MaF to reduce depth, leading to the result presented in Theorem 2.

Lemma 1. (Property of parity-controlled X gate) Under the condition that the input is a one-hot state, the parity-controlled X gate has the same effect as the quantum OR-controlled X gate.

Table III presents the circuit size, depth, and number of ancilla qubits required to execute the four steps of the algorithms, comparing both the cases with and without MaF. Due to the fact that  $d \leq 2^n$ , we can regard  $O(\log d)$  as O(n). In summary, both algorithms can be executed with the same size and number of ancilla qubits, O(dn) and O(d), respectively. The algorithm without MaF has a circuit depth of  $O(n \log d)$ . However, the depth can be reduced to a linear complexity in n by employing the MaF framework.

In Chapter II, we briefly introduce the required quantum gates, MaF, and then review the GQSP algorithm. The main algorithm is explained in detail in Chapter III. Finally, we discuss future work and summarize our research in Chapter IV.

## II. PRELIMINARIES

## A. Quantum gates

In this work, we will use the following gates: X gate, Hadamard gate,  $R_y$  gate, Controlled-NOT gate, Controlled- $R_y$  gate, Fredkin gate, Toffoli gate, multicontrolled single-target gate, and quantum fan-out gate.

TABLE IV. Elementary Quantum Gates.

| Operator                        | Gate               | Unitary   |
|---------------------------------|--------------------|---|
| Pauli-X (X)                     | x                  | $\begin{pmatrix} 0 & 1 \\ 1 & 0 \end{pmatrix}$  |
| Hadamard (H)                    | — н                | $\frac{1}{\sqrt{2}} \begin{pmatrix} 1 & 1 \\ 1 & -1 \end{pmatrix}$  |
| Y-axis Rotation $(R_y(\theta))$ | $ R_y(\theta)$ $-$ | $\begin{pmatrix} \cos \frac{\theta}{2} & -\sin \frac{\theta}{2} \\ \sin \frac{\theta}{2} & \cos \frac{\theta}{2} \end{pmatrix}$ |
| Controlled Not (CNOT)           |                    | $\begin{pmatrix} 1 & 0 & 0 & 0 \\ 0 & 1 & 0 & 0 \\ 0 & 0 & 0 & 1 \\ 0 & 0 & 1 & 0 \end{pmatrix}$                                |
| $\pi/8$ (T)                     | T_                 | $\begin{pmatrix} 1 & 0 \\ 0 & e^{\frac{i\pi}{4}} \end{pmatrix}'$  |

Table IV lists the elementary quantum gates used to construct all other required gates. The figures below outline the approaches for decomposing the Toffoli gate (Fig. 1), Fredkin gate (Fig. 2), and controlled- $R_y$  gate (Fig. 3). All of them have a constant depth.

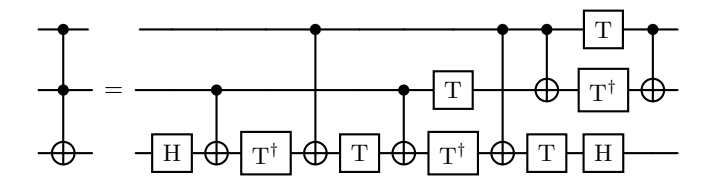


FIG. 1. Toffoli Gate

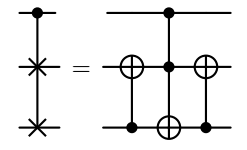


FIG. 2. Fredkin Gate

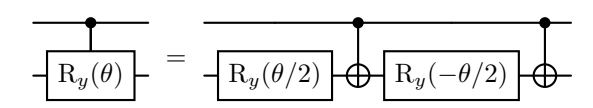


FIG. 3. controlled- $R_y$  Gate

Additionally, a multi-controlled rotation gate can be implemented by combining two multi-controlled Toffoli gates and two single-qubit rotation gates, as shown in Fig. 4. Similarly, as shown in Fig. 5, a quantum multi-OR-controlled single target X gate can be constructed using a multi-controlled Toffoli gate and the X gates. Consequently, the complexity of both gates depends on the n-Toffoli gate, whose size and depth are given in Lemma 2 (without ancilla) and Lemma 3 (with one ancilla)...

| Complexity          |       | Depth         |             |          |
|---------------------|-------|---------------|-------------|----------|
| Step                | Size  | Without MaF   | With MaF    | #Ancilla |
| GQSP                | O(d)  | $O(\log d)$   | $O(\log d)$ | O(d)     |
| One-hot encoding    | O(d)  | $O(\log^2 d)$ | $O(\log d)$ | O(d)     |
| Permutation         | O(dn) | $O(n \log d)$ | O(n)        | O(d)     |
| Garbage elimination | O(d)  | $O(n \log d)$ | O(n)        | O(d)     |
| Total               | O(dn) | $O(n \log d)$ | O(n)        | O(d)     |

TABLE III. Complexity summary for each step of our work.

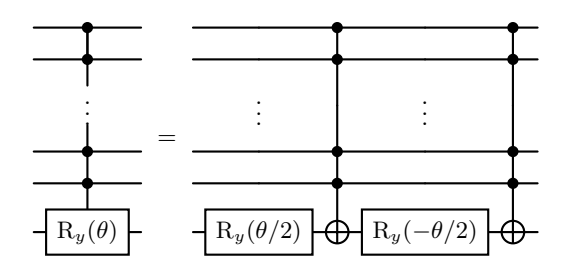


FIG. 4. control- $R_y$  Gate

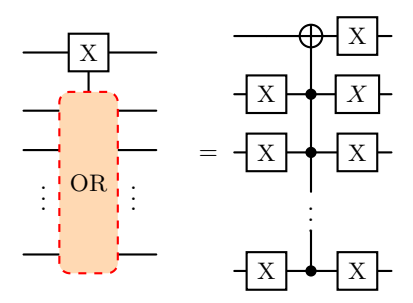


FIG. 5. A quantum multi-OR-controlled single target X gate (hereafter referred to as a quantum OR-controlled X gate), takes multiple control qubits and flips the target qubit if at least one of the control qubits is in the  $|1\rangle$  state, i.e. the OR of the control qubits is 1; otherwise, the target qubit remains unchanged.

Lemma 2. (Complexity of the *n*-Toffoli gat without ancilla [38]) With the gates set drawn from  $\{U(2),CNOT\}$ , *n*-Toffoli gate can be implemented by a quantum circuit of depth  $O(\log^2 n)$  and size O(n) using no ancilla qubit.

Lemma 3. (Complexity of the n-Toffoli gate with one ancilla [38]) With the gates set drawn from  $\{U(2),CNOT\}$ , n-Toffoli gate can be implemented by a quantum circuit of depth  $O(\log n)$  and size O(n) using one clean ancilla qubit.

The result of Lemma 2 allows us to complete the construction of the multi-controlled rotation gate with only logarithmic depth complexity. However, the quantum fan-out gate shown in Fig. 6 requires a linear depth to implement, which may increase the upper bound of the QSP circuit. As a result, we will discuss MaF in the next subsection to address this issue.

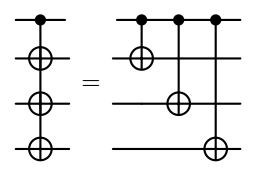


FIG. 6. Quantum fan-out Gate

## B. Quantum circuit with measurement and feedforward

In contrast to typical quantum circuits, a circuit with measurement and feedforward performs not only measurements at the end of the circuit to extract the result, but also intermediate measurements on selected qubits during the computation. The mid-circuit measurement outcomes are classically processed and used to control subsequent quantum operations. Inspired by the model presented in [36], we define the quantum circuit with measurement and feedforward (MaF) as follows:

Definition 2. (Quantum circuits with measurement and feedforward) Let  $\mathsf{MaF}(\mathcal{Q},\mathcal{C},l)$  be the class of circuits such that

- (1) every quantum layer implements a quantum circuit  $Q \in \mathcal{Q}$ ;
- (2) every classical layer implements a classical circuit  $C \in \mathcal{C}$ ;
- (3) there are *l* alternating layers of quantum and classical circuits:

- (4) after every quantum circuit Q a subset of the qubits is measured;
- (5) the classical circuits receive inputs from the measurement outcomes of previous quantum layers;
- (6) the classical circuits can control quantum operations in future layers.

We restrict our attention to a subclass of  $\mathsf{MaF}(\mathcal{Q},\mathcal{C},l)$ , where  $\mathcal{Q} = \mathsf{QPoly}(n)$ ,  $\mathcal{C} = \mathsf{NC}^1$ , and l = O(n). Throughout this work, we use  $\mathsf{MaF}$  to to abbreviate the class  $\mathsf{MaF}(\mathsf{QPoly}(n), \mathsf{NC}^1, O(n))$ . Here,  $\mathsf{QPoly}(n)$  denotes the class of quantum circuits with polynomial size, and  $\mathsf{NC}^1$  denotes the class of classical circuits with logarithmic depth and polynomial size. We refer to a circuit within this framework as a  $\mathsf{MaF}$  circuit.

Among various usages of  $\mathsf{MaF}$  circuit, one important use is in reducing circuit depth. We demonstrate how an n-qubit fan-out gate can be implemented using a constant depth circuit within  $\mathsf{MaF}$  framework, as shown in the following theorem.

Theorem 3. (Quantum fan-out gate within MaF framework [37]) An n-qubit quantum fan-out gate can be implemented by a constant-depth quantum circuit using n-1 ancilla qubits, and requires only a single layer of intermediate measurements.

The MaF circuit in Fig. 7 is an example of a 5-qubit quantum fan-out gate. It adds 4 ancilla qubits initialized in  $|0\rangle$ . The first quantum layer in  $\mathcal Q$  consists of a series of Hadamard and CNOT gates, followed by the mid-circuit measurements. The only classical layer C performs parallel XOR operations based on the measurement outcomes. Finally, the second quantum layer in  $\mathcal Q$ , which includes the final X and Z gates, is controlled by the classical output.

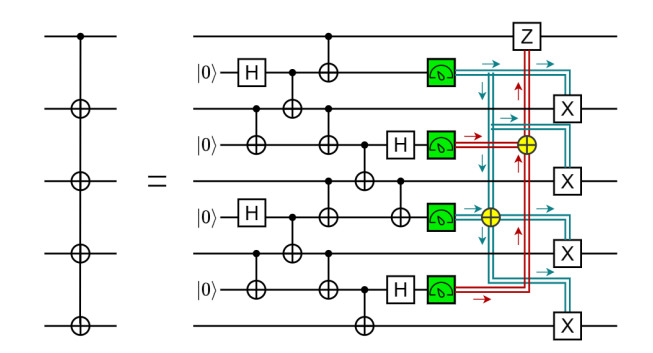


FIG. 7. Measurement-based implementation of the fanout gate

Notably, the fan-out gate requires only a single round of mid-circuit measurement, resulting in l=1 alternating layer of quantum and classical circuits. This structure enables its implementation on an arbitrary number of qubits with constant depth while maintaining linear size complexity, which is crucial to achieve SQSP circuit depth independent of the sparsity d.

#### C. Notation

In this paper, we adopt the following notation throughout the pseudocode. For a quantum register  $R \in \{A, B, C, D\}$ , the *i*th qubit in the R register is denoted as R(i). For example, A(i) refers to the *i*th qubit in the A register. When referring to a consecutive subset of qubits in a register, we use R(i, j) to denote the set of qubits from index i to j in the R register.

Building upon the notation defined above, we now introduce the expression of single-control quantum gates. A controlled-NOT gate acting on control qubit c and target qubit t is denoted as CNOT(c,t). Similarly, a controlled-SWAP gate acting on control qubit c and swapping the two target qubits  $t_1$  and  $t_2$  is written as  $CSWAP(c,t_1,t_2)$ . The notation FANOUT(c,t) represents a fan-out gate, where c is the control qubit and t is a set of target qubits. Both the control and target qubits in these gates are specified using the register notation introduced earlier. For example, FANOUT(B(i), A(j:k)) applies X gates to the jth through kth qubits in the A register, controlled by the ith qubit in the B register.

We next define multi-controlled quantum operations. Let CQ denote a classical register that stores the indices of control qubits. Based on this, we use the notation OR-C-X(R(CQ),t) to represent a quantum multi-OR-controlled single-target X gate, and Par-C-X(R(CQ),t) to represent a parity-controlled X gate, where t is the target qubit and the control qubits are those specified by the indices in CQ within the R register.

We also define the notation i(j) and  $q_i(j)$  to refer to the value of the jth bit in the binary representation of i and  $q_i$ , respectively. The bits are indexed from left to right. For instance, if i = 4 and its binary representation is 100, then i(0) = 1, i(1) = 0, and i(2) = 0.

## D. General quantum state preparation algorithm

The Grover-Rudolph algorithm [39] is a foundational method for general quantum state preparation (GQSP), and serves as the basis for many subsequent developments in this area. We briefly review this algorithm in this subsection. Nevertheless, the GQSP subroutine utilized in our SQSP algorithm differs from the original Grover-Rudolph method. Instead, we adopt a low-depth GQSP algorithm, as described in Theorem 5.

The General Quantum State Preparation problem aims to create an arbitrary quantum state of the form:

$$|\psi\rangle = \sum_{i=0}^{2^{n}-1} \alpha_{i} |i\rangle = \sum_{i=0}^{2^{n}-1} \alpha_{i} |i_{0}...i_{n-1}\rangle,$$
 (6)

where n denotes the number of qubits,  $\alpha_i$  denotes the amplitude corresponding to  $|i\rangle$ , and  $i_0...i_{n-1}$  is the binary representation of i.

Theorem 4. (Grover-Rudolph algorithmm [39]) With

the gate set drawn from  $\{U(2),CNOT\}$ , an arbitrary nqubit quantum state can be prepared with a circuit size  $O(n2^n)$ , depth<sup>2</sup>  $O(\log^2 n \cdot 2^n)$ .

To prepare the state  $|\psi\rangle$ , we need to implement a unitary  $U_{\psi}$  such that  $U_{\psi}|0\rangle = |\psi\rangle$ . The strategy is to decompose  $U_{\psi}$  into a series of simpler unitary transformations,  $U_{\psi} = U_{n-1}...U_0$ , where each unitary  $U_i$  performs the transformation  $U_i | \psi_i \rangle = | \psi_{i+1} \rangle$ . We define the intermediate states  $|\psi_i\rangle$  as follows:

$$|\psi_i\rangle = \sum_{k=0}^{2^i - 1} x_{i,k} |k\rangle |0\rangle^{\otimes n - i} = \sum_{k=0}^{2^i - 1} x_{i,k} |k_0...k_{i-1}\rangle |0\rangle^{\otimes n - i},$$
(7)

where  $k_0 \cdots k_{i-1}$  is the binary representation of k, and  $x_{i,k}$  is defined recursively by:

$$x_{i,k} = \sqrt{x_{i+1,2k}^2 + x_{i+1,2k+1}^2}$$
 (8)

with  $x_{n,k} = \alpha_k$ , for all k. Clearly,  $|\psi_0\rangle$  is the initial state  $|0\rangle^{\otimes n}$  of the algorithm, and  $|\psi_n\rangle$  corresponds to the desired output state  $|\psi\rangle$ .

Each unitary  $U_i$  can be implemented by applying a series of controlled rotations on the ith qubit, such that  $U_i$  transforms  $|\psi_i\rangle$  into  $|\psi_{i+1}\rangle$  as follows:

$$U_{i} | \psi_{i} \rangle$$

$$= U_{i} \sum_{k=0}^{2^{i}-1} x_{i,k} | k \rangle | 0 \rangle^{\otimes n-i}$$

$$= U_{i} \sum_{k=0}^{2^{i+1}-1} x_{i,k} | k \rangle | 0 \rangle^{\otimes n-i}$$

$$= \sum_{k=0}^{2^{i+1}-1} x_{i,k} | k \rangle \left( \cos \left( \frac{\theta_{i,k}}{2} \right) | 0 \rangle + \sin \left( \frac{\theta_{i,k}}{2} \right) | 1 \rangle \right) | 0 \rangle^{\otimes n-i-1}$$

$$= | \psi_{i+1} \rangle.$$
executing  $U_{n-1}$  on is successfully preparate depicted in Algorithm 1.

Input:  $| 0 \rangle^{n}$ ,  $\alpha_{k}$ , for  $\alpha_{k}$  in  $\alpha_{k}$  i

Here, the rotation angle  $\theta_{i,k}$  is defined as:

$$\theta_{i,k} = 2\arccos\left(\frac{x_{i+1,2k}}{x_{i,k}}\right),\tag{10}$$

To efficiently store and compute the intermediate amplitudes  $x_{i,k}$  and rotation angles  $\theta_{i,k}$ , we utilize a binary search tree (BST) data structure. The BST is constructed recursively, where the ith leaf node is assigned the amplitude  $x_{n,i} = \alpha_i$ . Each internal node stores the value  $x_{i,k}$  computed recursively using Eq. (8), along with its corresponding rotation angle  $\theta_{i,k}$  as defined in Eq.(10). The recursion proceeds from the leaf nodes up to the root, with each internal node's amplitude computed based on its two child nodes. As a result, the root node holds the value  $x_{0,0} = 1$  and the height of the BST will necessarily be n+1. Each edge from a parent node to its left child is labeled with a 0, while each edge to its right child is labeled with a 1. As a result, each path from the root to a leaf encodes a unique basis state in bianry, corresponding to the position of the amplitude  $\alpha_i$  in the final quantum state.

The rotation angles  $\theta_{i,k}$  stored in the BST serve as the parameters for constructing the quantum circuit. Specifically, the unitary  $U_i$  can be further decomposed into a sequence of  $2^i$  multi-controlled single-rotation gates of the form  $CR_y(\theta_{i,k})$ . Each  $CR_y(\theta_{i,k})$  gate is controlled by the first i qubits, and applies a y-axis rotation  $R_y(\theta_{i,k})$ on the i + 1th qubit when the control qubits are in the basis state  $|k\rangle$ , for  $k \in \{0, 1, \dots, 2^i - 1\}$ . The rotation acts as follows:

$$R_y(\theta_{i,k})|0\rangle = \cos\left(\frac{\theta_{i,k}}{2}\right)|0\rangle + \sin\left(\frac{\theta_{i,k}}{2}\right)|1\rangle.$$
 (11)

Once all  $CR_{\nu}(\theta_{i,k})$  operations for  $k = 0, \dots, 2^{i} - 1$  are applied, the unitary  $U_i$  completes its task. It adjusts the amplitude of the i + 1th qubit conditioned on the first i qubits, resulting in the updated state  $|\psi_{i+1}\rangle$ . This method allows the algorithm to build the desired superposition one qubit at a time, with the correct amplitudes encoded through the controlled rotations. Hence, after executing  $U_{n-1}$  on  $|\psi_{n-1}\rangle$ , the target state  $|\psi_n\rangle = |\psi\rangle$ is successfully prepared. The procedure explained above are depicted in Algorithm 1.

## ALGORITHM 1. Grover-Rudolph algorithm.

```
Input: |0\rangle^n, \alpha_k, for all k
```

(9)

```
1: for k \leftarrow 0 to 2^n-1 do
           x_{n,k} \leftarrow \alpha_k
 3: end for
 4: for i \leftarrow n - 1 to 0 do
           for k \leftarrow \text{to } 2^i - 1 \text{ do}
                 x_{i,k} \leftarrow \sqrt{x_{i+1,2k}^2 + x_{i+1,2k+1}^2}
                 \theta_{i,k} \leftarrow 2 \arccos\left(\frac{x_{i+1,2k}}{x_{i-k}}\right)
           end for
 8:
 9: end for
10: for i \leftarrow 0 to n-1 do
                                                  \triangleright Implement U_i in Eq.(9)
           for k \leftarrow 0 to 2^i - 1 do
                                                          \triangleright k_{(10)} = k_0..k_{i-1} (2)
11:
                 CR_y(\theta_{i,k_0...k_{i-1}})
           end for
13:
14: end for
```

Here, we present a simple example of a 3-qubit quantum state to illustrate general quantum state prepara-

$$\begin{split} |\psi\rangle &= \sqrt{0.05} \, |000\rangle + \sqrt{0.1} \, |001\rangle + \sqrt{0.03} \, |010\rangle + \sqrt{0.17} \, |011\rangle \\ &+ \sqrt{0.35} \, |100\rangle + \sqrt{0.09} \, |101\rangle + \sqrt{0.18} \, |110\rangle + \sqrt{0.03} \, |111\rangle \, . \end{split} \tag{12}$$

<sup>&</sup>lt;sup>2</sup> While the circuit depth was not provided in [39], we derive the depth by applying a recent low-depth construction of multicontrolled Toffoli gates.

The first step is to classically compute all the values of  $x_{i,k}$  by building the BST corresponding to  $|\psi\rangle$ , as depicted in Fig. 8.

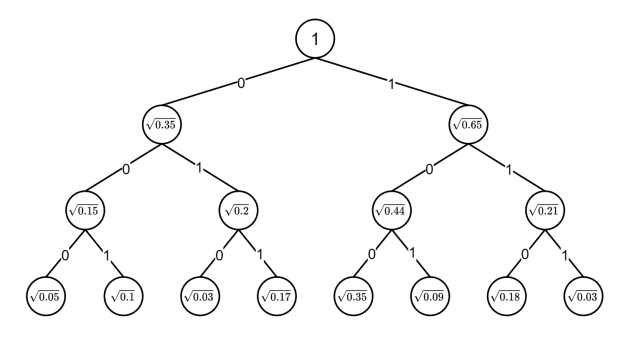


FIG. 8. Binary search tree with  $x_{i,k}$  for 3-qubit state  $|\psi\rangle$ 

We can then obtain the intermediate states  $|\psi_i\rangle$ :

$$\begin{aligned} |\psi_{0}\rangle &= |000\rangle \,, \\ |\psi_{1}\rangle &= (\sqrt{0.35} |0\rangle + \sqrt{0.65} |1\rangle) |00\rangle \,, \\ |\psi_{2}\rangle &= (\sqrt{0.15} |00\rangle + \sqrt{0.2} |01\rangle + \sqrt{0.44} |10\rangle + \sqrt{0.21} |11\rangle) |0\rangle \,, \\ |\psi_{3}\rangle &= |\psi\rangle \,. \end{aligned} \tag{13}$$

The rotation angles  $\theta_{i,k}$  can also be computed from the stored amplitudes using Eq. (10).

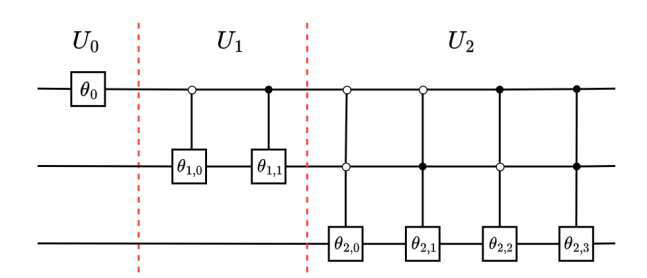


FIG. 9. The Grover-Rudolph circuit to prepare the 3-qubit state  $|\psi\rangle$ 

The circuit, as depicted in Fig. 9, is composed of  $U_0, U_1$  and  $U_2$ . The function of  $U_0$  is to map  $|000\rangle$  to  $|\psi_1\rangle$ . It can be done by rotating the first qubit with angle  $\theta_0$ . Similar to  $U_0$ ,  $U_1$  also applies a rotation on the second qubit, but the rotation angle depends on the first qubit. Since the first qubit has two possible states,  $|0\rangle$  and  $|1\rangle$ ,  $U_1$  has two different angles corresponding to each case. In the same way,  $U_2$  consists of four different rotation gates with controlled gates acting on the first two qubits. The Grover-Rudolph procedure sequentially rotates each qubit with specific angles, eventually leading to the final state  $|\psi_3\rangle \equiv |\psi\rangle$ .

However, due to the exponential circuit depth required by Grover-Rudolph's algorithm, it cannot be completed quickly. To address this, other studies have proposed using additional ancilla qubits to parallelize the algorithm and reduce the circuit depth. Theorem 5. (Low-depth GQSP algorithm [40]) With the gates set drawn from  $\{U(2),CNOT\}$ , an arbitrary n-qubit quantum state can be prepared with a circuit depth O(n) and  $O(2^n)$  ancilla qubits.

# III. SPARSE QUANTUM STATE PREPARATION ALGORITHM

In this section, we present algorithm for preparing any n-qubit d-sparse quantum state

$$|\phi\rangle = \sum_{i=0}^{d-1} \alpha_i |q_i\rangle. \tag{14}$$

using O(d) ancilla qubits. The primary goal is to reduce the circuit depth for SQSP. The algorithm is made up of four steps: GQSP, one-hot encoding, permutation, and garbage elimination, as shown in the Eq.(15).

$$|0\rangle^{\otimes n} |0\rangle^{\otimes 4d}$$

$$\stackrel{1}{\to} \sum_{i=0}^{d-1} \alpha_{i} |i\rangle |0\rangle^{\otimes n - \lceil \log d \rceil} |0\rangle^{\otimes 4d}$$

$$\stackrel{2}{\to} \sum_{i=0}^{d-1} \alpha_{i} |i\rangle |0\rangle^{\otimes n - \lceil \log d \rceil} |e_{i}\rangle |0\rangle^{\otimes 3d}$$

$$\stackrel{3}{\to} \sum_{i=0}^{d-1} \alpha_{i} |q_{i}\rangle |e_{i}\rangle |0\rangle^{\otimes 3d}$$

$$\stackrel{4}{\to} \sum_{i=0}^{d-1} \alpha_{i} |q_{i}\rangle |0\rangle^{\otimes 4d}$$

$$= |\phi\rangle |0\rangle^{\otimes 4d}.$$
(15)

The first step, GQSP, uses the GQSP algorithm of Theorem 5 on the first  $\lceil \log d \rceil$  qubits to generate d amplitudes, corresponding to  $\alpha_0$  through  $\alpha_{d-1}$  of the target state  $|\phi\rangle$ . In the second step, to enable parallel execution of subsequent procedures, we perform one-hot encoding that maps the d basis states to d ancilla qubits. The third step, permutation, uses the one-hot state as control to permute all amplitudes to their correct positions. Finally, after resetting the ancilla qubits, the algorithm is complete and the target state  $|\phi\rangle$  is obtained. In the following, we will walk through the details of 4 steps.

#### A. General quantum state preparation

The first step is to construct a  $\lceil \log d \rceil$ -qubit dense state  $|\phi'\rangle$ :

$$|\phi'\rangle = \sum_{i=0}^{d-1} \alpha_i |i\rangle. \tag{16}$$

To reduce the circuit depth, we adopt the GQSP algorithm described in Theorem 5, which prepares  $|\phi'\rangle$  using  $O(\log d)$  circuit depth and O(d) ancilla qubits.

## B. One-hot encoding

For convenience, we refer to the state  $|\phi'\rangle |0\rangle^{n-\lceil \log d \rceil}$  as the A register. The 2d ancilla qubits are divided into two d-qubit registers, referred to as the B register and the C register.

To further reduce the circuit depth with ancilla qubits, we map the first  $\lceil \log d \rceil$ -qubits of register A,  $|i\rangle$ , to the B register as one-hot encoding:

$$\sum_{i=0}^{d-1} \alpha_{i} \underbrace{|i\rangle |0\rangle^{n-\lceil \log d \rceil}}_{A} \underbrace{|0\rangle^{\otimes d}}_{B} \underbrace{|0\rangle^{\otimes d}}_{C} \qquad (17)$$

$$\longrightarrow \sum_{i=0}^{d-1} \alpha_{i} |i\rangle |0\rangle^{n-\lceil \log d \rceil} |e_{i}\rangle |0\rangle^{\otimes d},$$

where  $|e_i\rangle$  denotes the quantum state in which the *i*th qubit is  $|1\rangle$ , while all other qubits are  $|0\rangle$ , known as the one-hot encoding of *i*.

We can implement this transformation using an X gate and CSWAP gates. As an example, Fig. 10 illustrates a circuit for executing the one-hot encoding when n = 5, d = 8. The procedure begins by applying an X gate to the first qubit of the B register, resulting in the state  $|e_0\rangle$ . Next, we will use the A register to control a sequence of CSWAP gates that move the  $|1\rangle$  to its correct position. For  $j = 0 \sim \lceil \log d \rceil - 1$ , the jth qubit in A register controls  $2^j$  CSWAP gates, with their first target qubits uniquely corresponding to all possible 11) positions. These possible positions are, in fact, the  $2^{j}$  target qubits of the CSWAP gates controlled by the j-1th qubit in A register. Each of CSWAP gates controlled by jth qubit can be discussed in two cases. If the jth qubit is  $|0\rangle$ , it means that this qubit does not alter the value of i, and thus, the state in the B register does not need to change. If the control qubit is  $|1\rangle$ , it indicates the addition of a value  $2^{\lceil \log d \rceil - j - 1}$ , so a CSWAP must be applied to move  $|1\rangle$  forward by  $2^{\lceil \log d \rceil - j - 1}$  positions. Consequently, the second target qubits of all the CSWAP gates are positioned  $2^{\lceil \log d \rceil - j - 1}$ th qubits after the first target qubits.

There are  $2^j$  swap gates controlled by the jth qubit for  $j = 0 \sim \lceil \log d \rceil - 1$ , so both the circuit size and circuit depth are O(d). In Algorithm 2, we provide the pseudocode for encoding one-hot state.

## ALGORITHM 2. One-hot Encoding.

Input: 
$$\sum_{i=0}^{d-1} \alpha_i \underbrace{|i\rangle |0\rangle^{\otimes n - \lceil \log d \rceil}}_{A} \underbrace{|0\rangle^{\otimes d}}_{B}$$
Output: 
$$\sum_{i=0}^{d-1} \alpha_i |i\rangle |0\rangle^{\otimes n - \lceil \log d \rceil} |e_i\rangle$$

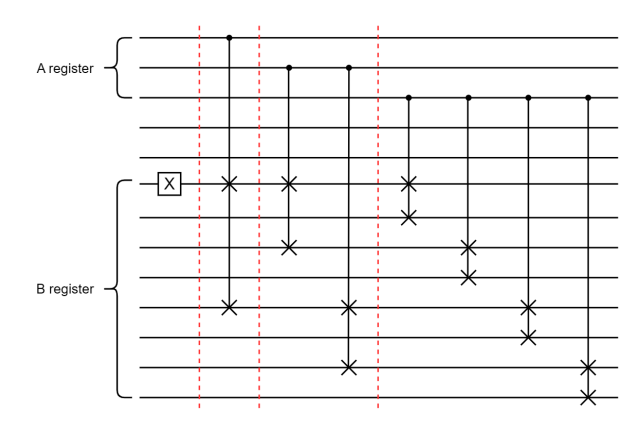


FIG. 10. A simple example of one-hot encoding for n = 5, d = 8

- 1: Flip the first qubit of the B register.
- 2: for  $j \leftarrow 0$  to  $\lceil \log d \rceil 1$  do  $\triangleright$  Designate the jth qubit as the control qubit.
- 3: **for**  $i \leftarrow 0$  to  $2^j 1$  **do**
- 4:  $\operatorname*{CSWAP}_{2\lceil \log d \rceil j 1 \rceil )} \operatorname{CSWAP}(\mathbf{A}(j), \, \mathbf{B}(i \cdot 2^{\lceil \log d \rceil j}), \, \mathbf{B}(i \cdot 2^{\lceil \log d \rceil j} +$
- 5: **end for**
- 6: end for

To reduce the circuit depth, we allow all the CSWAP gates controlled on the same qubit to execute in parallel [The for loop in lines 3 - 5 in Algorithm 2]. This is achieved by using only CNOT gates to copy enough control qubits into the C register, enabling the parallel execution of all controlled gates on the C register. The copy circuit is illustrated in Fig. 11. In each layer of the circuit, CNOT gates parallel copy the state to fresh ancilla qubits, doubling the number of copies with constant depth. The process of copying a single qubit k times requires only  $O(\log k)$  circuit depth.

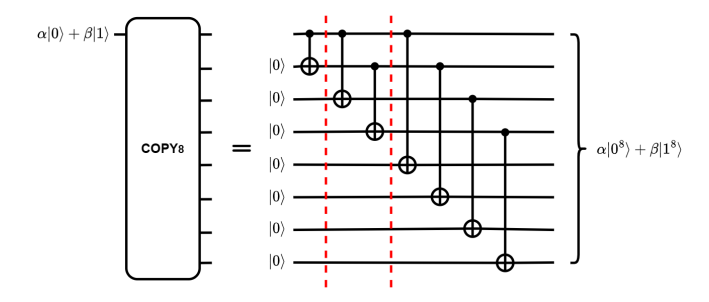


FIG. 11. An example of a circuit that performs single qubit copying

# ALGORITHM 3. One-hot Encoding with $\mathcal{O}(d)$ ancilla qubits.

Input: 
$$\sum_{i=0}^{d-1} \alpha_{i} \underbrace{|i\rangle |0\rangle^{\otimes n-\lceil \log d \rceil}}_{A} \underbrace{|0\rangle^{\otimes d}}_{B} \underbrace{|0\rangle^{\otimes d}}_{C}$$
Output: 
$$\sum_{i=0}^{d-1} \alpha_{i} |i\rangle |0\rangle^{\otimes n-\lceil \log d \rceil} |e_{i}\rangle |0\rangle^{\otimes d}$$

```
1: Flip the first qubit of the B register.
    for j \leftarrow 0 to \lceil \log d \rceil - 1 do
 3:
         CNOT(A(j), C(0))
         for k \leftarrow 0 to j-1 do
 4:
             for l \leftarrow 0 to 2^k - 1 do
 5:
                  CNOT(C(l), C(l+2^k))
 6:
             end for
 7:
         end for
 8:
         for i \leftarrow 0 to 2^j - 1 do
 9:
              CSWAP(C(i), B(i \cdot 2^{\lceil \log d \rceil - j}), B(i \cdot 2^{\lceil \log d \rceil - j} +
10:
    2\lceil \log d \rceil - j - 1 \rceil
         end for
11:
         for k \leftarrow j-1 to 0 do
12:
             for l \leftarrow 2^k - 1 to 0 do
13:
                  CNOT(C(l), C(l+2^k))
14:
             end for
15:
         end for
16:
         CNOT(A(j), C(0))
17:
18: end for
```

Originally, the  $2^j$  CSWAP gates controlled by the jth qubit require a circuit depth of  $O(2^j)$ . By copying the control qubit to the C register, the CSWAP gates can be controlled by C register in parallel, reducing their circuit depth to a constant. The copying process has a circuit depth O(j). Summing over all j from 0 to  $\lceil \log d \rceil - 1$ , the total circuit depth of one-hot encoding is  $O(\lceil \log d \rceil^2)$ . The pseudocode is described in Algorithm 3.

When the MaF circuit is allowed, the copy operation can be implemented more efficiently using constant-depth fan-out gates, as depicted in Fig. 7. Since there are at most  $\frac{d}{2}$  SWAP gates controlled by the same qubit, the fan-out gate requires at most  $\frac{d}{2}$  target qubits and  $\frac{d}{2}$  ancilla qubits. Therefore, the C register provides sufficient qubits to perform the copy operation. As a result, Step 2 can be completed with circuit depth  $O(\log d)$ , while maintaining a circuit size of O(d). We give an example of Parallel CSWAP gates in Fig. 12 and pseudocode for encoding the one-hot state with MaF circuit in Algorithm 4.

## ALGORITHM 4. One-hot Encoding with MaF.

```
Input: \sum_{i=0}^{d-1} \alpha_{i} \underbrace{|i\rangle |0\rangle^{\otimes n - \lceil \log d \rceil}}_{A} \underbrace{|0\rangle^{\otimes d}}_{B} \underbrace{|0\rangle^{\otimes d}}_{C}
Output: \sum_{i=0}^{d-1} \alpha_{i} |i\rangle |0\rangle^{\otimes n - \lceil \log d \rceil} |e_{i}\rangle^{\otimes d} |0\rangle^{\otimes d}
1: Flip the first qubit of the B register.
```

```
2: for j \leftarrow 0 to \lceil \log d \rceil - 1 do
3: FANOUT(A(j), C(0: 2^j - 1))
4: for i \leftarrow 0 to 2^j - 1 do
5: CSWAP(C(j), B(i \cdot 2^{\lceil \log d \rceil - j}), B(i \cdot 2^{\lceil \log d \rceil - j} + 2^{\lceil \log d \rceil - j - 1}))
6: end for
7: FANOUT(A(j), C(0: 2^j - 1))
8: end for
```

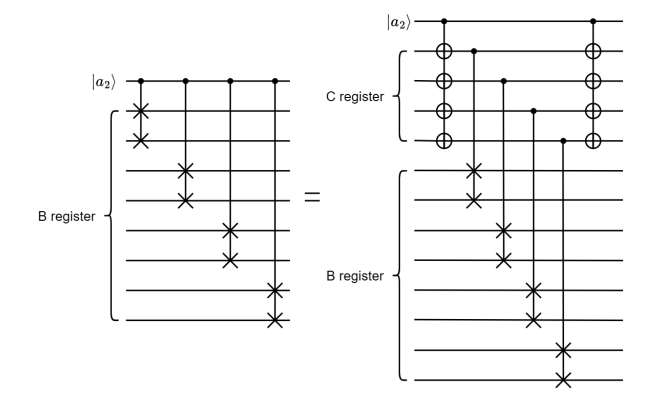


FIG. 12. An example of a circuit that performs CSWAP gates in parallel

### C. Permutation

In Step 3, we map the n qubits in the A register to their correct positions, as shown in the transformation below:

$$\sum_{i=0}^{d-1} \alpha_i \underbrace{|i\rangle |0\rangle^{\otimes n - \lceil \log d \rceil}}_{A} \underbrace{|e_i\rangle}_{B} \underbrace{|0\rangle^{\otimes d}}_{C} \longrightarrow \sum_{i=0}^{d-1} \alpha_i |q_i\rangle |e_i\rangle |0\rangle^{\otimes d}.$$
(18)

By controlling on the one-hot state, we can identify and flip the properly qubits in the A register one by one. Suppose we are mapping the jth qubit in the A register. If the jth qubit of  $|i\rangle|0\rangle^{\otimes n-\lceil\log d\rceil}$  differs from that of  $|q_i\rangle$ , a CNOT gate is applied with the ith qubit of the B register as the control and the jth qubit of the A register as the target. As long as the control qubit is in the state  $|1\rangle$ , it indicates that the corresponding jth qubit in the A register is incorrect and will be flipped by the target gate to reach the expected value.

Processing the jth qubit of  $|e_i\rangle$  require at most d CNOT gates with disjoint control but the same target qubit, which costs a high circuit depth of O(d). To minimize the circuit depth, we adopt a quantum OR-controlled X gate to perform the flip operation in parallel, as shown in Fig. 5. The target of the quantum OR-controlled X gate is the jth qubit of the A register. For each basis state  $|q_i\rangle$ , if its jth qubit differs from that of the A register, then the ith qubit of the B register is included as a control in the OR-controlled X gate. As long as at least one control qubit is in the  $|1\rangle$  state, the target qubit will be flipped.

Since there are at most d control qubits, flipping any qubit in the A register requires a circuit of size O(d) and depth  $O(\log d)$ . Therefore, mapping all n qubits to their correct positions costs circuit size O(dn) and depth  $O(n \log d)$ . The pseudocode is described in Algorithm 5.

## ALGORITHM 5. Permutation.

$$\begin{split} &\textbf{Input: } \sum_{i=0}^{d-1} \alpha_i \underbrace{|i\rangle \, |0\rangle^{\otimes n - \lceil \log d \rceil}}_{A} \underbrace{|e_i\rangle}_{B} \underbrace{|0\rangle^{\otimes d}}_{C} \\ &\textbf{Output: } \sum_{i=0}^{d-1} \alpha_i \, |q_i\rangle \, |e_i\rangle \, |0\rangle^{\otimes d} \end{split}$$

Due to the property established in Lemma 1, the parity-controlled X gate can be used in place of the quantum OR-controlled X gate to achieve the same effect.

For example, consider the transformation of 5-qubit 8-sparsity quantum state:

$$\begin{aligned} |\psi\rangle &= (\alpha_{0} |000\rangle + \alpha_{1} |001\rangle + \alpha_{2} |010\rangle + \alpha_{3} |011\rangle + \alpha_{4} |100\rangle + \alpha_{5} |101\rangle + \alpha_{6} |110\rangle + \alpha_{7} |111\rangle) |00\rangle \\ \longrightarrow \\ \alpha_{0} |01001\rangle + \alpha_{1} |01110\rangle + \alpha_{2} |10001\rangle + \alpha_{3} |10010\rangle \\ + \alpha_{4} |10111\rangle + \alpha_{5} |11010\rangle + \alpha_{6} |11101\rangle + \alpha_{7} |11110\rangle \,. \end{aligned}$$
(19)

We can sequentially apply five parity-controlled X gates to the five qubits in the A register, each controlled by the one-hot state, as Fig. 13.

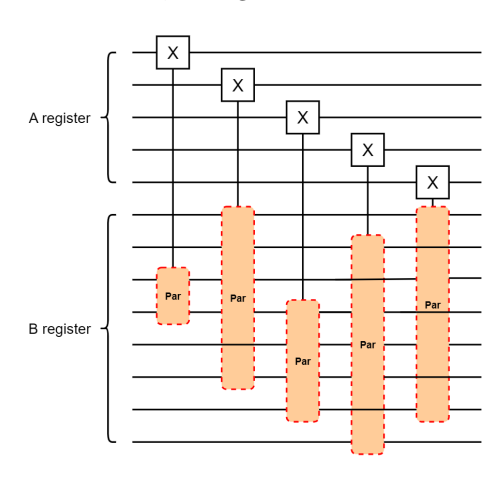


FIG. 13. An example circuit for implementing permutation

As shown in [41], parity-controlled X gates and fanout gates are related by conjugation with a layer of Hadamard gates. This directly leads to the following corollary:

Corollary 1. (Quantum parity-controlled X gate with MaF) The n-qubit parity-controlled X gate can be implemented by a constant-depth quantum circuit using n an-

cilla qubits. This implementation requires the Hadamard gates and a constant-depth fan-out gate, which is realized using a circuit with measurement and feedforward(MaF), as described in Theorem 3. Figure. 14 provides a simple example of this construction.

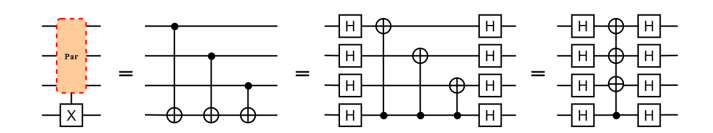


FIG. 14. The parity-controlled X gate can be constructed from a fan-out gate and Hadamard gates.

Because the parity-controlled X gate involves at most d control qubits, implementing the fan-out gate with MaF requires, in the worst case, d ancilla qubits. These ancilla qubits can be provided by the C register.

Since Step 3 involves n parity-controlled X gates, each with constant depth, the overall depth complexity of Step 3 is O(n). Furthermore, as the fan-out gate has a complexity of linear size, the permutation circuit complexity is O(dn). We document the pseudocode of the permutation circuit implementation in Algorithm 6.

## ALGORITHM 6. Permutation with MaF.

Input: 
$$\sum_{i=0}^{d-1} \alpha_{i} \underbrace{\ket{i} \ket{0}^{\otimes n - \log d}}_{A} \underbrace{\ket{e_{i}}}_{B} \underbrace{\ket{0}^{\otimes d}}_{C}$$
Output: 
$$\sum_{i=0}^{d-1} \alpha_{i} \ket{q_{i}} \ket{e_{i}} \ket{0}^{\otimes d}$$

```
1: for j \leftarrow 0 to n-1 do
        CQ \leftarrow \emptyset
2:
        for i \leftarrow 0 to d-1 do
3:
            if i(j) \neq q_i(j) then
4:
                 CQ \leftarrow CQ \bigcup \{i\}
5:
            end if
6:
7:
        end for
        Par-C-X(B(CQ), A(j))
8:
9: end for
```

## D. Garbage elimination

In this step, we use four registers: the A register and the B register as before, the C register for 2d qubits, and the D register for d qubits. This step aims to eliminate the one-hot encoding  $|e_i\rangle$  in the B register:

$$\sum_{i=0}^{d-1} \alpha_i \underbrace{|q_i\rangle}_{A} \underbrace{|e_i\rangle}_{B} \underbrace{|0\rangle^{\otimes 2d}}_{C} \underbrace{|0\rangle^{\otimes d}}_{D} \longrightarrow \sum_{i=0}^{d-1} \alpha_i |q_i\rangle |0\rangle^{\otimes d} |0\rangle^{\otimes 2d} |0\rangle^{\otimes d}.$$

$$(20)$$

Before designing the circuit, we first construct a binary search tree (BST) representing the states  $|q_i\rangle$  for all i. Each path from the root to a leaf node corresponds to a specific  $|q_i\rangle$ . The edge at the jth layer denotes the

value of the jth qubit of  $|q_i\rangle$ : an edge leading to the left child represents  $|0\rangle$ , and an edge leading to the right child represents  $|1\rangle$ . A branch node is defined as a node with two child nodes. The kth branch node refers to the kth branch node in the BST, indexed by traversing from the root to the leaves, and from left to right within each layer, where  $k=1,2,\ldots,d-1$ . The BST has height n,d leaf nodes, and d-1 branch nodes in total. It follows that each layer contains at most  $\frac{d}{2}$  branch nodes.

We realize the transformation defined in Eq.(20) through the following steps:

$$\sum_{i=0}^{d-1} \alpha_{i} |q_{i}\rangle |e_{i}\rangle |0\rangle^{\otimes 2d} |0\rangle^{\otimes d}$$

$$\xrightarrow{4.1} \sum_{i=0}^{d-1} \alpha_{i} |q_{i}\rangle |e_{i}\rangle \bigotimes_{k=1}^{d-1} |f(q_{i},k)\rangle |0\rangle^{\otimes d}$$

$$\xrightarrow{4.2} \sum_{i=0}^{d-1} \alpha_{i} |q_{i}\rangle |0\rangle^{\otimes d} \bigotimes_{k=1}^{d-1} |f(q_{i},k)\rangle |0\rangle^{\otimes d}$$

$$\xrightarrow{4.3} \sum_{i=0}^{d-1} \alpha_{i} |q_{i}\rangle |0\rangle^{\otimes d} |0\rangle^{\otimes 2d} |0\rangle^{\otimes d}$$

$$= |\phi\rangle.$$
(21)

We define the 2-qubit state  $|f(q_i, k)\rangle$  in (21) based on the kth branch node in the BST, such that

$$|f(q_i,k)\rangle = \begin{cases} |10\rangle\,, & \text{if } q_i \text{ takes the left branch at the} \\ & k\text{th branch node.} \\ |01\rangle\,, & \text{if } q_i \text{ takes the right branch at the} \\ & k\text{th branch node.} \\ |00\rangle\,, & \text{if the path of } q_i \text{ does not pass} \\ & \text{through the } k\text{th branch node.} \end{cases}$$

In Step 4.1, the BST is recorded in the C register. This allows Step 4.2 to eliminate the garbage state in the B register by controlling with the C register. Finally, the C register is reset using the same procedure as in Step 4.1. We now show the implementation of the process step by step and analyze its circuit complexity.

## 1. BST encoding

In the first substep, for each basis state  $|q_i\rangle$  in the superposition, the kth branch node of the BST is recorded in the 2-qubit state  $|f(q_i,k)\rangle$  in the C register. This process is performed in parallel over all i, while the records for each k are generated sequentially in the order of branch node indices. Specifically, if  $|q_i\rangle$  passes through the left (right) subtree of the kth branch node, we set  $|f(q_i,k)\rangle = |10\rangle$  ( $|01\rangle$ ). If  $|q_i\rangle$  does not pass through the jth branch node, then we set  $|f(q_i,j)\rangle = |00\rangle$  and no action is needed. Since there are d-1 branch nodes and each requires 2 qubits to encode its status, the C register contains sufficient ancilla qubits to store the traversal information for all paths.

To begin recording the information of the first branch node, we start from the 0th layer of the BST and search layer by layer until we reach the first branch node. Suppose that it is located at the jth layer. We then record this branch node in the first two qubits of the C register, denoted by  $|f(q_i, 1)\rangle$ . This is done by applying an X gate to the first qubit and then a CSWAP gate controlled by the jth qubit of the A register. The possible values of  $|f(q_i, 1)\rangle$  are  $|10\rangle$  or  $|01\rangle$ :  $|10\rangle$  means that the path of  $q_i$  in the BST passes through the left subtree of the first branch node, while  $|01\rangle$  means that it passes through the right subtree.

Next, we proceed to record the branch nodes in order, traversing from the root to the leaves and from left to right at each layer. Suppose we are currently recording the kth branch node B at the jth layer, and let  $|B\rangle$  denote the 2-qubit state that records B. We define the parent branch node of B, denoted by B', as the nearest branch node along the path from B to the root of the BST. Since branch nodes are recorded in traversal order, we can ensure that B' has already been recorded before B. To begin recording B, we first apply a CNOT gate, where the target is the first qubit of  $|B\rangle$ , and the control is one of the two qubits that encode B'. There are two cases to consider:

- (1) If the 2-qubit state recording B' is  $|00\rangle$ , it means that B' is not on the path of  $q_i$ . Therefore, B is not on the path of  $q_i$  either.
- (2) If the 2-qubit state recording B' is  $|10\rangle$  or  $|01\rangle$ , then the path of  $q_i$  traverses the left or right subtree of B', respectively.

Accordingly, if B lies in the left subtree of B', we use the first qubit of B' as the control; otherwise, we use the second qubit. In this way, the target qubit is flipped if and only if the path of  $q_i$  passes through B, resulting in  $|B\rangle = |10\rangle$ . Otherwise, the state remains  $|00\rangle$ , indicating that  $q_i$  does not pass through B.

Subsequently, similar to the process of recording the first branch, we apply a CSWAP gate to the two qubits of  $|B\rangle$ , controlled by the jth qubit of the A register. If the target qubits are in the state  $|00\rangle$ , this indicates that B is not on the path of  $q_i$ , and the CSWAP gate has no effect on  $|B\rangle$ . On the other hand, if the target qubits are in the state  $|10\rangle$ , the effect of the CSWAP depends on the value of the control qubit: if the control qubit is  $|0\rangle$ , the target qubits remain unchanged, and the state  $|B\rangle$  stays as  $|10\rangle$ , signifying that  $q_i$  takes the left branch at B; if the control qubit is  $|1\rangle$ , the target qubits are swapped, resulting in the state  $|01\rangle$ , which indicates that  $q_i$  takes the right branch at B. Finally, this completes the recording of the kth branch node, where  $|B\rangle = |f(q_i, k)\rangle$ , as described in Eq. (21).

Here, we present a simple example of BST encoding for a 3-qubit 5-sparsity quantum state:

$$|\psi\rangle = \alpha_0 |001\rangle + \alpha_1 |010\rangle + \alpha_2 |011\rangle + \alpha_3 |110\rangle + \alpha_4 |110\rangle.$$
 (23)

First, we need to build the BST corresponding to  $|\psi\rangle$ , as depicted in Fig. 15.

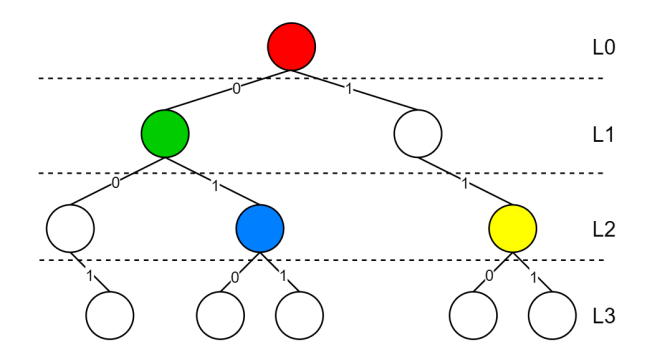


FIG. 15. Binary search tree for  $|\psi\rangle$ . The colored nodes represent the branch nodes.

We then record the branch nodes layer by layer, proceeding from the top to the bottom of the BST, and from left to right within each layer. As depicted in Fig. 16, the circuit consists of three layers. The first layer records the first branch node using an X gate followed by a CSWAP gate. In the second layer, the second branch node is recorded based on the information from its parent—the root node—which has already been recorded. Finally, the third layer records all the branch nodes at the third level of the BST in sequence, using the same method.

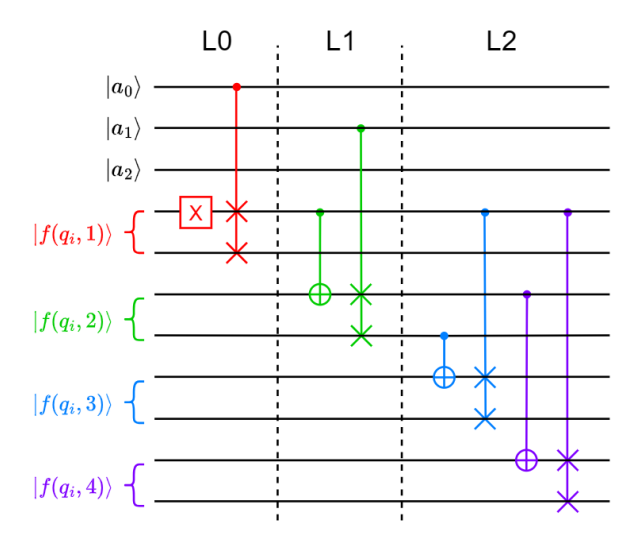


FIG. 16. Circuit for recording the binary search tree (BST) encoding without MaF.

Consider the process of recording all b(j) branch nodes located at the jth layer of the BST. All the CNOT gates can be executed in parallel since both their control and target qubits are mutually disjoint. However, although the CSWAP gates also act on distinct target qubits, they are all controlled by the same jth qubit of the A register. As a result, these CSWAP gates cannot be executed in parallel, which increases the circuit depth.

To reduce the circuit depth, we copy the control qubit

into b(j) ancilla qubits in the D register, enabling all the CSWAP gates to be applied simultaneously within the same layer. The resulting circuit depth thus depends on the depth of the copy operation. By using the copy circuit shown in Fig. 11, all branch nodes at the jth layer can be recorded in parallel with a circuit size of O(b(j)) and a circuit depth of  $O(\log b(j))$ . If MaF circuits are allowed, the copy operation can be performed even more efficiently using constant-depth fan-out gates, as illustrated in Fig. 7. Consequently, the recording of all b(j) branch nodes at the jth layer can be accomplished in constant circuit depth.

Since the number of branch nodes in any given layer is at most  $\frac{d}{2}$ , we have b(j) = O(d) for each j. In summary, recording the entire BST requires a circuit depth of  $O(n\log d)$  without MaF, and O(n) when using the MaF framework. In both cases, the total circuit size remains O(d). The pseudocode for the full process under the MaF framework is presented in Algorithm 7. Here, the notation b(j) denotes the number of branch nodes in the jth layer of the BST, and PB(k) refers to the index of the parent branch node of the kth branch node in the BST. Using the recorded information from this step, we will eliminate the one-hot encoding  $e_i$  in the next step.

## ALGORITHM 7. BST recording with MaF.

```
\overline{\mathbf{Input:} \sum_{i=0}^{d-1} \alpha_i \underbrace{|q_i\rangle}_{A} \underbrace{|e_i\rangle}_{B} \underbrace{|0\rangle^{\otimes 2d}}_{C} \underbrace{|0\rangle^{\otimes d}}_{D}}
Output: \sum_{i=0}^{d-1} \alpha_i |q_i\rangle |e_i\rangle \bigotimes_{k=1}^{d-1} |f(q_i,k)\rangle |0\rangle^{\otimes d}
  1: firstBranch \leftarrow true
  2: k \leftarrow 1
  3: for j \leftarrow 0 to n-1 do
           if firstBranch then
  5:
                firstBranch \leftarrow false
                X(C(0))
  6:
                CSWAP(A(i),C(0),C(1))
  7:
           else if b(j) \neq 0 then
  8:
                for i \leftarrow 1 to b(j) do
  9:
                     if (k + i)th branch node in its parent
 10:
      branch node's left subtree then
                           CNOT(C(2PB(k+i)-2),C(2(k+i-1))
 11:
 12:
                           CNOT(C(2PB(k+i)-1),C(2(k+i-1))
 13:
                     end if
 14:
                end for
 15:
                FANOUT(A(j),D(0:b(j)-1))
 16:
                for i \leftarrow 1 to b(j) do
 17:
                      CSWAP(D(i),C(2(k+i-1)),C(2(k+i)-1))
 18:
```

## 2. Garbage elimination

FANOUT(A(j),D(0:b(j)-1))

19:

20:

21:

22:

23: end for

end for

end if

 $k \leftarrow k+b(i)$ 

In this substep, we identify the value of  $|q_i\rangle$  via the C register to flip the correct qubit in the B register. This can be done in parallel and requires only constant depth.

It is known that each one-hot encoding  $|e_i\rangle$  corresponds to a state  $|q_i\rangle$ , and each  $|q_i\rangle$  corresponds to a path from the root to a leaf in the BST. Suppose we want to eliminate the state  $|e_t\rangle$ . The main approach is to apply a CNOT gate to flip the tth qubit in the B register. We can first identify the lowest branch node on the path corresponding to  $|e_t\rangle$ . If the path goes through the left subtree of this branch node, the control qubit of the CNOT gate is the first qubit of the two qubits recording this branch node; otherwise, it is the second qubit. When the B register is in the state  $|e_t\rangle$ , the control qubit will necessarily act, ultimately transforming  $|e_t\rangle$  to  $|0\rangle^{\otimes d}$ . We can execute the process of eliminating  $|e_t\rangle$  for all  $t=0\sim d-1$  in parallel, because the control and target qubits for all the CNOT gates are distinct. It is obvious that the depth complexity is O(1) and size complexity is O(n) in this step. Algorithm 8 presents the procedure for eliminating the garbage state. The notation LB(i) refers to the index of the lowest branch node on the path corresponding to  $q_i$  in the BST.

## ALGORITHM 8. Garbage Elimination.

Input: 
$$\sum_{i=0}^{d-1} \alpha_{i} |q_{i}\rangle |e_{i}\rangle \bigotimes_{k=1}^{d-1} |f(q_{i},k)\rangle |0\rangle^{\otimes d}$$
Output: 
$$\sum_{i=0}^{d-1} \underbrace{\alpha_{i} |q_{i}\rangle}_{A} \underbrace{|0\rangle^{\otimes d}}_{B} \underbrace{\bigotimes_{k=1}^{d-1} |f(q_{i},k)\rangle}_{C} \underbrace{|0\rangle^{\otimes d}}_{D}$$

```
1: for i \leftarrow 0 to d-1 do
2: Find the lowest branch node LB on the path corresponding to |e_i\rangle
3: if the path go through the left subtree of LB then
4: \text{CNOT}(\text{C}(2\text{LB}(i)\text{-}2),\text{B}(i))
5: else
6: \text{CNOT}(\text{C}(2\text{LB}(i)\text{-}1),\text{B}(i))
7: end if
8: end for
```

## 3. Reset C register

As soon as the garbage state is eliminated, the C register can be rapidly deallocated. The method is similar to Step 4.1. Additionally, the size and depth complexity is the same as in Step 4.1.

After completing Step 4, the garbage state is eliminated and the desired state  $|\phi\rangle$  is obtained. Without using MaF, the process requires a circuit depth of  $O(n \log d)$ , while with MaF, the depth can be reduced to O(n). The size complexity is O(d) in both cases.

## E. Proof

Having introduced the four steps of the SQSP algorithm, we now integrate these procedures to derive and

formally prove the overall complexity results. Specifically, we summarize and prove Theorem 1 and Theorem 2, which correspond to the cases without and with the MaF circuit, respectively.

Proof of Theorem 1. (SQSP algorithm) The SQSP algorithm begins with the input state  $|0\rangle^{\otimes n}$ . In the Step 1, a  $\lceil \log d \rceil$ -qubit state is prepared using a low-depth GQSP algorithm that encodes the target amplitudes. This step requires a circuit size of O(d) and a depth of  $O(\log d)$ .

The Step 2 constructs a one-hot state, enabling parallel execution of the subsequent permutation step. This is achieved by applying CSWAP gates to move the  $|1\rangle$  to the correct position. To reduce the circuit depth, ancilla qubits and the copy operations are used to parallelize the CSWAP operations. As a result, the circuit depth is compressed to  $O(\log^2 d)$  with total circuit size O(d).

In the Step 3, OR-C-X gates are controlled in parallel by the one-hot states corresponding to all basis states, encoding each qubit sequentially to its correct value. This permutation step realizes the target state with a circuit size of O(dn) and depth  $O(n \log d)$ .

Finally, the Step 4 eliminates the one-hot encoding. This is done by first constructing a BST of the target state and then recording the branch node information based on the BST. Similar to second step, a copy operation is used here to reduce the circuit depth. The CNOT gates are then applied to reset the one-hot state in parallel. The circuit size is O(dn) and depth  $O(n \log d)$  in this step.

By combining these four steps, an arbitrary n-qubit dsparsity quantum state can be efficiently prepared, with
a total circuit size of O(dn), depth  $O(n \log d)$  and O(d)ancilla qubits.

Proof of Theorem 2. (SQSP algorithm with a MaF circuit) The structure of this algorithm largely follows the same steps as in Prf. 1 and achieves the same circuit size and ancilla complexity. We highlight here the key differences that arise when using a MaF circuit, which allows fan-out operations to be implemented in constant depth and thus reduces the overall depth complexity.

The Step 1, GQSP, remains unchanged, with circuit size and depth being O(d) and  $O(\log d)$ , respectively.

Since fan-out gates can perform the copy operation, the copy circuits in both Step 2 and Step 4 can be replaced with constant-depth fan-out gates. This reduces their depths from  $O(\log^2 d)$  and  $O(n \log d)$  to  $O(\log d)$  and O(n), respectively, while maintaining the same circuit sizes of O(d) and O(dn).

In Step 3, under the assumption that the input is a one-hot state, the OR-C-X gates behave equivalently to Par-C-X gates. Since Par-C-X gates can be implemented using Hadamard gates and fan-out gates, the circuit depth can be reduced from  $O(n \log d)$  to O(n), while maintaining the same circuit size of O(dn).

In summary, the overall circuit depth can be reduced from  $O(n \log d)$  to O(n), making it independent of the sparsity d, while maintaining a circuit size of O(dn) and

O(d) ancilla qubits.

#### IV. CONCLUSION

In this work, we propose two efficient algorithms to prepare arbitrary sparse quantum state, with a focus on optimizing circuit depth under a limited number of ancilla gubits. The core idea is to first generate the correct amplitudes, and then relocate each amplitude to its designated position. In the first algorithm, we prepare each qubit sequentially rather than constructing the full basis states one by one. By using O(d) ancilla qubits, we leverage copy operations and one-hot encoding to parallelize the computation. As a result, the overall circuit has size O(dn), depth  $O(n \log d)$ , and requires O(d) ancilla qubits. To further reduce the circuit depth, the second algorithm incorporates measurement and feedforward. By performing certain operations conditionally based on mid-circuit measurement outcomes, the circuit depth can be reduced to O(n) while maintaining the same circuit size and ancilla requirements.

For future work, it would be interesting to explore approaches that offer different trade-offs between ancilla qubits and circuit depth. Additionally, it is worth investigating more efficient state preparation algorithms adapted to different scaling of sparsity d with respect to the number of qubits n. Another open question is to establish lower bounds on the circuit depth required for quantum state preparation under measurement-and-feedforward (MaF) architectures.

### ACKNOWLEDGEMENT

This work is supported by NSTC QC project under Grant no. 114-2119-M-001-002- and 113-2112-M-007-043-.

# APPENDIX: LOCAL OPERATION AND CLASSICAL COMMUNICATION

Many studies on LOCC and its related applications have been published over the past decade. [42–44] In the following, we present an introduction to LOCC [45] and LAQCC [36], and provides a detailed comparison with MaF.

Local operation and classical communication (LOCC) is a fundamental concept in quantum information the-

ory used to describe operations on distributed quantum systems under specific constraints. It consists of two key components:

- (1) Local operations Each party can only perform operations on their local quantum subsystem. These operations include measurements, unitary transformations, additions of ancilla, and discarding or preparing new quantum states.
- (2) Classical communication Parties can exchange measurement outcomes through classical channels but cannot directly share quantum information, such as quantum states or entanglement. The purpose of classical communication is to coordinate their actions such that another local operation is performed, conditioned on the information received.

Inspired by the concept of LOCC in quantum information, an LOCC circuit architecture is proposed, where the circuit is constructed with geometrically local gates, and these local gates are controlled by classical information computed from previous measurement results. Such a circuit is referred to as an LOCC-circuit.

Local alternating quantum classical computations (LAQCC), similar to LOCC, is a architecture that incorporates mid-circuit measurements and real-time feed-forward operations. In this framework, quantum and classical operations are alternated in a controlled manner, and each qubit arranged in a grid can only interact with their immediate neighbors. The main distinction between LOCC and LAQCC is that LAQCC restricts quantum operators to constant depth, classical operators to logarithmic depth, and allows at most a constant number of alternations between them. From this, we can conclude that any LAQCC-circuit has constant total quantum depth.

Since the LOCC-circuits also incorporate the mid-circuit measurements, they fall within the category of circuits with MaF. The key difference is that, under the LOCC framework, each quantum gate is allowed to interact only with adjacent qubits, whereas circuits with MaF are not subject to this constraint. We note that the fanout gate shown in Fig. 7 also operates within the LOCC framework. However, in this work, we utilize the fan-out gates where the control and target qubits are not necessarily adjacent. Moreover, other operations in the circuit are not strictly local either. As a result, the SQSP circuits we propose fall under the circuit with MaF category rather than being constrained to LOCC.

<sup>[1]</sup> P. W. Shor, SIAM Rev., 303 (1996).

<sup>[2]</sup> L. K. Grover, in *Proceedings of the twenty-eighth annual ACM symposium on Theory of computing* (Assoc. Comput. Mach., Pennsylvania, 1996) pp. 212–219.

<sup>[3]</sup> M. Cerezo, A. Arrasmith, R. Babbush, S. C. Benjamin,

S. Endo, K. Fujii, J. R. McClean, K. Mitarai, X. Yuan, L. Cincio, et al., Nat. Rev. Phys. 3, 625 (2021).

<sup>[4]</sup> S. Woerner and D. J. Egger, Npj Quantum Inf. 5, 15 (2019).

<sup>[5]</sup> V. Markov, C. Stefanski, A. Rao, and C. Gonciulea, A

- generalized quantum inner product and applications to financial engineering, arXiv:2201.09845 [quant-ph].
- [6] A. M. Dalzell, A shortcut to an optimal quantum linear system solver, arXiv:2406.12086v1 [quant-ph].
- [7] D. Jennings, M. Lostaglio, S. Pallister, A. T. Sornborger, and Y. Subaşı, Efficient quantum linear solver algorithm with detailed running costs, arXiv:2305.11352v1 [quantph].
- [8] I. Alabdulmohsin, H. Maennel, and D. Keysers, The impact of reinitialization on generalization in convolutional neural networks, arXiv:2109.00267 [quant-ph].
- [9] X. Sun, G. Tian, S. Yang, P. Yuan, and S. Zhang, IEEE Trans. CAD 42, 3301 (2023).
- [10] M. Plesch and Č. Brukner, Phys. Rev. A 83, 032302 (2011).
- [11] A. Shukla and P. Vedula, Quantum Inf. Process. 23, 38 (2024).
- [12] I. F. Araujo, C. Blank, I. C. Araújo, and A. J. da Silva, IEEE Trans. CAD 43, 161 (2024).
- [13] F. Mozafari, Y. Yang, and G. De Micheli, in 27th Asia and South Pacific Design Automation Conference (ASP-DAC),2022 (IEEE, Virtual Conference, 2022) pp. 460– 465.
- [14] N. Gisin and H. Bechmann-Pasquinucci, Phys. Lett. A 246, 1 (1998).
- [15] A. Frisk Kockum, V. Macrì, and F. Nori, Phys. Rev. A 98, 062327 (2018).
- [16] W. Cottrell, B. Freivogel, D. M. Hofman, and S. F. Lokhande, J. High Energy Phys. (online) 2019, 1 (2019).
- [17] W. Dür, G. Vidal, and J. I. Cirac, Phys. Rev. A 62, 062314 (2000).
- [18] A. Bärtschi and S. Eidenbenz, Deterministic preparation of dicke states, in *Fundamentals of Computation Theory*, edited by L. A. Gasieniec, J. Jansson, and C. Levcopoulos (Springer, Cham, 2019) pp. 126–139.
- [19] B. Chor and B. A. Coan, IEEE Trans. Software Eng. SE-11, 531 (1985).
- [20] N. Gleinig and T. Hoefler, in 2021 58th ACM/IEEE Design Automation Conference (DAC) (IEEE, San Francisco, 2021) pp. 433–438.
- [21] F. Mozafari, G. De Micheli, and Y. Yang, Phys. Rev. A 106, 022617 (2022).
- [22] N. M. Tubman, C. Mejuto-Zaera, J. M. Epstein, D. Hait, D. S. Levine, W. Huggins, Z. Jiang, J. R. McClean, R. Babbush, M. Head-Gordon, and K. B. Whaley, Postponing the orthogonality catastrophe: efficient state preparation for electronic structure simulations on quantum devices, arXiv:1809.05523v1 [quant-ph].
- [23] D. Ramacciotti, A. I. Lefterovici, and A. F. Rotundo, Phys. Rev. A 110, 032609 (2024).
- [24] T. M. de Veras, L. D. da Silva, and A. J. da Silva, Quantum Inf. Process. 21, 204 (2022).
- [25] X.-M. Zhang, T. Li, and X. Yuan, Phys. Rev. Lett. 129, 230504 (2022).
- [26] R. Mao, G. Tian, and X. Sun, Phys. Rev. A 110, 032439 (2024).

- [27] T. M. De Veras, I. C. De Araujo, D. K. Park, and A. J. Da Silva, IEEE Trans. Comput. 70, 2125 (2020).
- [28] A. Gonzales, R. Herrman, C. Campbell, I. Gaidai, J. Liu, T. Tomesh, and Z. H. Saleem, in 2024 IEEE International Conference on Quantum Computing and Engineering (QCE) (IEEE, Montreal, 2024) pp. 616–617.
- [29] J. Luo and L. Li, Nearly optimal circuit size for sparse quantum state preparation, arXiv:2406.16142v2 [quantph].
- [30] R. Acharya, D. A. Abanin, L. Aghababaie-Beni, I. Aleiner, T. I. Andersen, M. Ansmann, F. Arute, K. Arya, A. Asfaw, N. Astrakhantsev, et al., Nature 638, 920 (2024).
- [31] C. H. Bennett, G. Brassard, C. Crépeau, R. Jozsa, A. Peres, and W. K. Wootters, Phys. Rev. Lett. 70, 1895 (1993).
- [32] M. Iqbal, N. Tantivasadakarn, T. M. Gatterman, J. A. Gerber, K. Gilmore, D. Gresh, A. Hankin, N. Hewitt, C. V. Horst, M. Matheny, et al., Commun. Phys. 7, 205 (2024).
- [33] W. Zi, J. Nie, and X. Sun, Constant-depth quantum circuits for arbitrary quantum state preparation via measurement and feedback, arXiv:2503.16208 [quant-ph].
- [34] D. Maslov, Phys. Rev. A **76**, 052310 (2007).
- [35] S. Ubaru, I. Y. Akhalwaya, M. S. Squillante, K. L. Clarkson, and L. Horesh, Quantum topological data analysis with linear depth and exponential speedup, arXiv:2108.02811 [quant-ph].
- [36] H. Buhrman, M. Folkertsma, B. Loff, and N. M. Neumann, Quantum 8, 1552 (2024).
- [37] E. BBäumer and S. Woerner, Phys. Rev. Res. 7, 023120 (2025).
- [38] J. Nie, W. Zi, and X. Sun, Quantum circuit for multi-qubit toffoli gate with optimal resource (2024), arXiv:2402.05053v1 [quant-ph].
- [39] L. Grover and T. Rudolph, Creating superpositions that correspond to efficiently integrable probability distributions (2002), arXiv:quant-ph/0208112v1 [quant-ph].
- [40] K. Gui, A. M. Dalzell, A. Achille, M. Suchara, and F. T. Chong, Quantum 8, 1257 (2024).
- [41] C. Moore, Quantum circuits: Fanout, parity, and counting, arXiv:quant-ph/9903046v3 [quant-ph].
- [42] E. Chitambar, D. Leung, L. Mančinska, M. Ozols, and A. Winter, Everything you always wanted to know about locc (but were afraid to ask), in *Communications in Mathematical Physics*, Vol. 328, edited by L. A. Gasieniec, J. Jansson, and C. Levcopoulos (Springer, Cham, 2014) pp. 303–326.
- [43] L. Piroli, G. Styliaris, and J. I. Cirac, Phys. Rev. Lett. 133, 230401 (2024).
- [44] Y. Yan, M. Ma, Y. Zhou, and X. Ma, Phys. Rev. Lett. 134, 170601 (2025).
- [45] L. Piroli, G. Styliaris, and J. I. Cirac, Phys. Rev. Lett. 127, 220503 (2021).